Journal of Materials Chemistry C

Accepted Manuscript

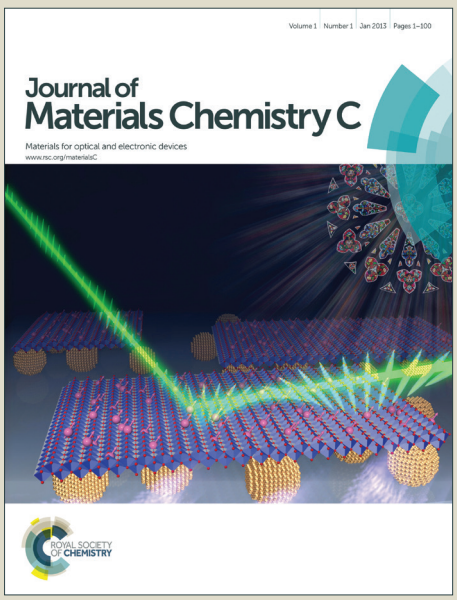

ROYAL SOCIETY OF CHEMISTRY

www.rsc.org/materialsC

Temperature-Dependent Reaction between Trimethylaluminum and Poly(methyl methacrylate) during Sequential Vapor Infiltration: Experimental and *ab initio* Analysis

Erinn C. Dandley, Craig D. Needham, Philip S. Williams, Alexandra H. Brozena,

Christopher J. Oldham and Gregory N. Parsons

Department of Chemical and Biomolecular Engineering

North Carolina State University, Raleigh NC 27695

Abstract

Vapor-phase, metal-containing organic compounds can diffuse into polymers and modify the material composition and structure. In this work, using a sequential vapor infiltration process based on atomic layer deposition chemistry, we combine *in situ* Fourier transform infrared transmission and quartz crystal microbalance experiments with *ab initio* quantum chemical modeling analysis to evaluate and identify likely reaction mechanisms when poly(methyl methacrylate) (PMMA) thin films are exposed to trimethylaluminum (TMA) vapor. We find that TMA readily diffuses into the PMMA, where it physisorbs onto ester carbonyl units (C=O) to form a metastable C=O···Al(CH_3)$_3$ adduct structure that desorbs at moderate temperatures (< ~ 100°C). The Lewis-acidic TMA withdraws charge from the C=O, shifting its stretching frequency from 1732 cm^{-1} in untreated PMMA to 1670 cm^{-1} after TMA exposure. At higher temperatures IR results show a new feature near 1568 cm^{-1} that is stable, even upon exposure to water vapor, indicating covalent bond formation. Based on known TMA/polymer reaction mechanisms and *ab initio* model results, we propose that at T > 100°C, TMA reacts with PMMA to form covalent resonant C=O···Al-O-C bonding units, and does not form -O-C-O-Al(CH_3) as previously hypothesized. This mechanistic insight will help elucidate other polymer/Lewis acid vapor reactions and could enable to new applications for sequential vapor infiltration processes.

Introduction

Several active research groups currently explore polymer modification by vapor-phase, metal-organic reagents to understand reactions that alter material surface and bulk structure as well as functionality.[1–8] Improved understanding of vapor infusion and reaction mechanisms will help expand the use of current methods, and will lead to discovery of novel approaches or process schemes to enable new and broader applications. For example, Sequential Vapor Infiltration (SVI) proceeds by repeatedly exposing a polymer, or other material, to a vapor reactant, usually a metal-organic species, in a heated reactor environment. After the reagent vapor flows into the reactor the deposition chamber is closed for a set "hold" time, increasing the net reactant exposure. Sequential exposures are separated by an inert gas purge to remove vapor byproducts and renew the reactant concentration. Co-reactants, such as water to produce metal oxide products, are also delivered either as an additional step within the reactant/inert gas sequence, or after completing the desired number of reactant infusion/purge cycles. This approach has grown from atomic layer deposition (ALD), which uses sequential, self-limiting reactant exposure steps to deposit conformal and uniform thin films on surfaces with monolayer precision.[9–11] Variations on the process take different names, including multiple pulse infiltration[1,2] and sequential infiltration synthesis.[5,6] Multiple pulse infiltration also uses a hold step after precursor exposure, whereas sequential infiltration synthesis typically uses co-reactant exposures after each precursor step, without hold steps.[8]

Infiltration and reaction involving trimethylaluminum (TMA) vapor and the polymer poly(methyl methacrylate) (PMMA), the latter in a thin film [9,12] or block co-polymer (BCPs) such as polystyrene-*block*-poly(methyl methacrylate) (PS-*b*-PMMA)[5,6], is a commonly studied system. PMMA has reactive functional groups and a relatively large free volume. TMA is a common reagent for ALD of Al_2O_3; its small size and high reactivity make it a good candidate to study vapor infusion and reaction processes. Several recent studies show that TMA exposure to PS-*b*-PMMA BCPs lead to selective reaction within

the PMMA which, upon subsequent plasma oxidation, produces a solid template of the original PMMA that can be used for pattern transfer and lithography.[5,6]

Even with this interest in vapor infusion, the detailed chemical mechanisms associated with the reaction remain uncertain. A recent study from our group[12] using *in situ* infrared transmission (IR) showed that TMA infusion and reaction depend strongly on the nature of the starting polymer structure. Moreover, based on changes in the IR, we hypothesized mechanisms for TMA/polymer reactions that included covalent bond formation between TMA and PMMA at moderate process temperature (80°C).

In this article we present more detailed results including temperature dependent IR, quartz crystal microbalance (QCM) mass uptake, and quantum chemical modeling analysis. We also show that at moderate temperatures TMA forms a non-covalent, metastable adduct coordinating to the PMMA carbonyl unit. The TMA either desorbs from this coordinated complex under purge conditions or subsequently reacts, most readily at higher temperatures, to form a covalent Al-O bonding structure that remains present after water exposure. New insight from this analysis will be helpful to understand reaction products and mechanisms for this and other vapor-phase metal-organic interactions with polymers.

Experimental Procedures

Chemicals and materials:

Poly(methyl methacrylate) (Fluka Analytical, MW 97,000) and trimethylaluminum (Strem Chemicals, min 98% pure) were used as received. TMA was co-reacted with deionized water after a specified number of TMA doses. The reactor was purged with high purity nitrogen gas (Machine & Welding Supply Co) that was further purified with a Entegris GateKeeper located directly upstream from the reactor input. PMMA was spun-cast onto silicon substrates (University Wafers, P-type, <100>) by first dissolving PMMA into toluene (Fischer Scientific) from one to eight weight percent PMMA. Silicon

wafers were cleaned with acetone (Fischer Scientific) and dried by spinning at 2000 rpm for one minute. The surface of the silicon was flooded with PMMA solution and then spun at 2000 rpm for one minute. The sample was then heated on a hot plate at 200°C for two minutes to remove toluene.

Sequential vapor infiltration (SVI)

SVI was used to infiltrate the PMMA thin film. Briefly, the sample was placed into a custom made, viscous-flow, hot-walled, vacuum reactor described previously.[3,4,13] The reactor was kept at roughly 800 mTorr, and operated at temperatures between 45 and 150 °C. TMA was introduced into the reactor and held by closing all ports into and out of the reactor for a set time period. The reactor was then purged with N_2 gas. This was repeated *n* times followed by a dose of water and a final purge. We anticipate that the final water step would help form a protective barrier on the outside of the polymer-TMA composite to block the rapid reaction of trapped TMA with atmospheric water. The typical dosing scheme for these experiments was a 1 second TMA dose, 60 second hold, and 30 second purge, all repeated as many times as desired. This is followed by a 1 second dose of water and a 45 second final purge. This scheme is denoted as [(1/60/30) $\times$ *n* + (1/45)]. For the duration of this article a "TMA dose" will refer to one TMA dose, hold and purge step and will be reported as a number of repeats of the TMA dose (*n*).

Characterization:

PMMA layer thickness was determined by spectroscopic ellipsometry (J.A. Woollam Co., Inc) and by profilometry (Veeco Dektak 150). Mass gain was quantified using an *in situ* quartz crystal microbalance. For QCM analysis, 50 nm PMMA films were cast onto quartz crystals (gold plated, 6 MHz resonant frequency, Inficon). They were then affixed to a crystal drawer (Inficon) with conductive silver epoxy (MG Chemicals). The crystal drawer was then inserted into the sensor head and placed into the reactor. The set up was allowed to equilibrate at process temperature overnight. The oscillating

frequency of the crystal was recorded every 150 milliseconds and converted into a mass gain using the Sauerbrey equation.

Changes in chemical bonding were measured using an *in situ* Fourier transform infrared spectrophotometer (Nicolet 6700 FTIR) incorporated into a custom built viscous flow vacuum reactor.[3,4,12,14] Samples were cast onto IR transparent silicon wafers. The sample was prebaked in the reactor to a temperature of 140°C for 30 minutes under vacuum and flowing N_2 gas to remove any volatile species from the PMMA. The system was then cooled to the infiltration temperature and allowed to equilibrate for 30 minutes. Spectra were taken after 10, 50, 100, and 150 TMA doses as well as after water dosing. After the prescribed number of TMA doses the chamber was purged for two minutes and then closed off. Gates to the IR windows were then opened and 200 spectra were obtained at a resolution of 4 cm^{-1} in the frequency range of 4000 to 400 cm^{-1}. An MCT-A detector was used through CsI IR windows.

Quantum chemistry analysis

Optimized geometries and frequencies of PMMA, TMA, and the PMMA–TMA coordination complex were calculated using Gaussian09.[15] The B3LYP Density Functional Theory method was implemented because of its ability to accurately predict frequency data through the use of a scaling factor. All calculations were performed using a 6-31G++(d,p) basis set. This basis set provides suitable accuracy and rapid system output. As is commonly done with the B3LYP functional[16,17] we used a multiplication factor of 0.961 to adjust the calculated frequencies to better replicate the experimental values. The as-calculated and adjusted values are reported. We also employed Gaussview[18] to construct the model structures and view the calculated vibrations to identify modes in the experimental spectra. All simulations used methyl trimethylacetate as a model molecule for PMMA due to its

structural similarity to one PMMA repeat unit. It has been shown that methyl trimethylacetate has a similar carbonyl stretching frequency to PMMA.[19]

Results

In situ FTIR and QCM

Figure 1 shows *in situ* FTIR results following 150 TMA doses on PMMA films between 45 and 150°C. Each spectrum was collected from a separate experiment, starting each time with a fresh, spun-

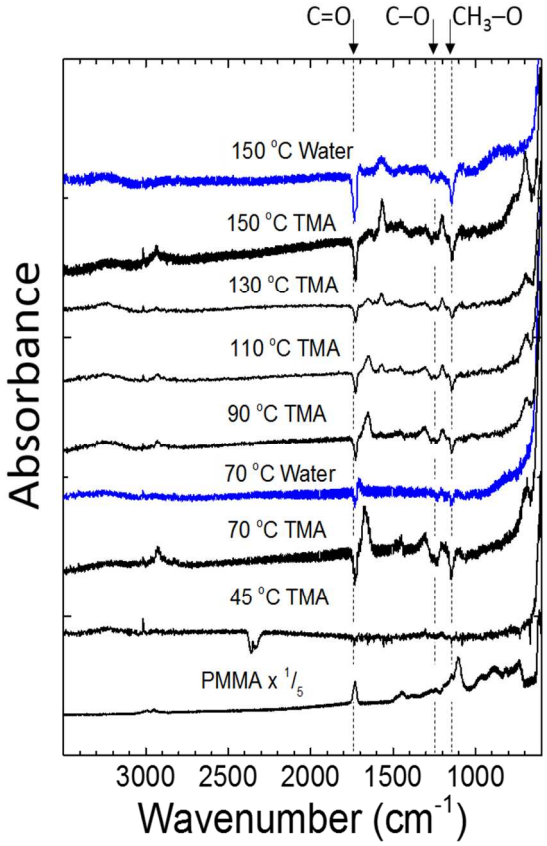

Figure 1. *In situ* FTIR spectra collected after 150 TMA doses on 170 nm thick PMMA films on silicon. The spectra are shown in differential mode, relative to the starting PMMA. Two spectra collected after TMA + water at 70 and 150 °C are also included, and similarly referenced to the starting PMMA.

cast PMMA film. Spectra are shown in differential mode relative to the starting PMMA substrate. The starting PMMA spectrum shows peaks at 1732, 1260 and 1143 cm^{-1} (noted with dashed lines in Figure 1). The spectra show notable changes upon TMA exposure, especially in the region between 1100 and 1800 cm^{--1}. The magnitude of mode intensity change upon TMA exposure could depend on temperature, TMA partial pressure, exposure time, purge time, and starting layer thickness. Therefore, to address the effect of temperature, we fixed the pressure, exposure, purge time and substrate thickness (< ± 1%) for all spectra collected. With these considerations, the distinct mode changes in Figure 1 reasonably relate to different extents of reaction, or different reaction products produced at the temperatures studied.

Previously, we reported *in situ* IR analysis of reactions between TMA and various polymer thin films, including PMMA, at a fixed temperature (80°C); spectra were similar to those at 70 and 90°C shown here in Figure 1. We note here that PMMA modes can be seen for C=O stretching at 1732 cm^{-1}, and for C-O stretching in the =C-O- and -O-CH_3 units near 1260 and 1143 cm^{-1} (*vide infra*). Consider first the effect of TMA exposure at 70°C on the IR results in Figure 1. After 150 TMA exposure steps, the difference spectrum shows negative going modes at 1732, 1260 and 1143 cm^{-1}, and positive going modes at 1670, 1305, and 1200 cm^{-1}, indicating significant modification of the C=O and C-O bonds. We previously observed and quantified changes in IR signature upon TMA exposure, concluding that TMA readily diffuses and reacts in the polymer bulk. That work also reported the changes in the C=O and C-O modes,[12] where we assigned the mode near 1600 cm^{-1} (at 1670 cm^{-1} in Figure 1) to reaction between TMA and the C=O forming O-C-O-Al units. Based on experimental and modeling results discussed in detail below, we revise this interpretation and assign the mode at 1670 cm^{-1} to TMA complexed to the ester C=O in a Lewis acid/base adduct.[20] Physisorbed TMA will also indirectly affect the non-carbonyl oxygen of the ester moiety via resonance, resulting in shifts in the C-O modes.

Considering the data in Figure 1 collected at T= 45°C, there is much less change in the IR modes than at 70°C. For T >70°C the 1670 cm^{-1} mode also appears but it is less intense at increased

temperature. Moreover, at T = 110°C a small mode becomes visible at 1568 cm^{-1} and it intensifies as the reaction temperature increases to 150°C. The identity of the 1568 cm^{-1} mode is discussed in detail below.

In addition to spectra collected after TMA exposure, Figure 1 shows IR traces collected after water exposure (referenced to the starting PMMA) following TMA at 70 and 150°C. At 70°C, the TMA/water exposure sequence produced only small net changes in the PMMA features, indicating that the water step reverses or removes much of the change that occurred during the TMA step. TMA in the film will react with water to create Al-O clusters, consistent with the small broad feature near 820 cm^{-1} due to Al-O stretching. The TMA/water sequence at 150 °C produces a very different outcome. The TMA step produces a negative-going peak at 1732 cm^{-1} and a positive-going mode at 1568 cm^{-1}, and it remains present after the water step (i.e. the spectra labeled "TMA" and "Water" at 150 °C look relatively similar). These results suggest the TMA forms a reversible product with the PMMA at low temperature (removed by water exposure), but at high temperature TMA reacts with the polymer to form a stable covalent product (not strongly modified by water). The =C-O- and -O-CH_3 modes at 1260 and 1143 cm^{-1} in the starting PMMA show similar trends. At 70°C, the TMA exposure leads to changes that are largely reversed by the water dose, whereas at high temperature, the TMA leads to changes that are relatively stable upon water exposure (i.e. the spectra labeled "TMA" and "Water" are very different at low temperature, but are more similar at 150°C). In the Discussion section below, we consider possible PMMA–TMA reaction mechanisms and covalent bond products that can account for these IR results.

To further explore the reaction between TMA and PMMA, we performed quartz crystal microbalance measurements during repeated TMA exposures on 50 nm spun-cast PMMA films at various reaction temperatures; results are shown in Figure 2. The QCM response over 60 TMA doses (Fig. 2a) show rapid net mass uptake during the first ~10 doses followed by slower uptake. For the three

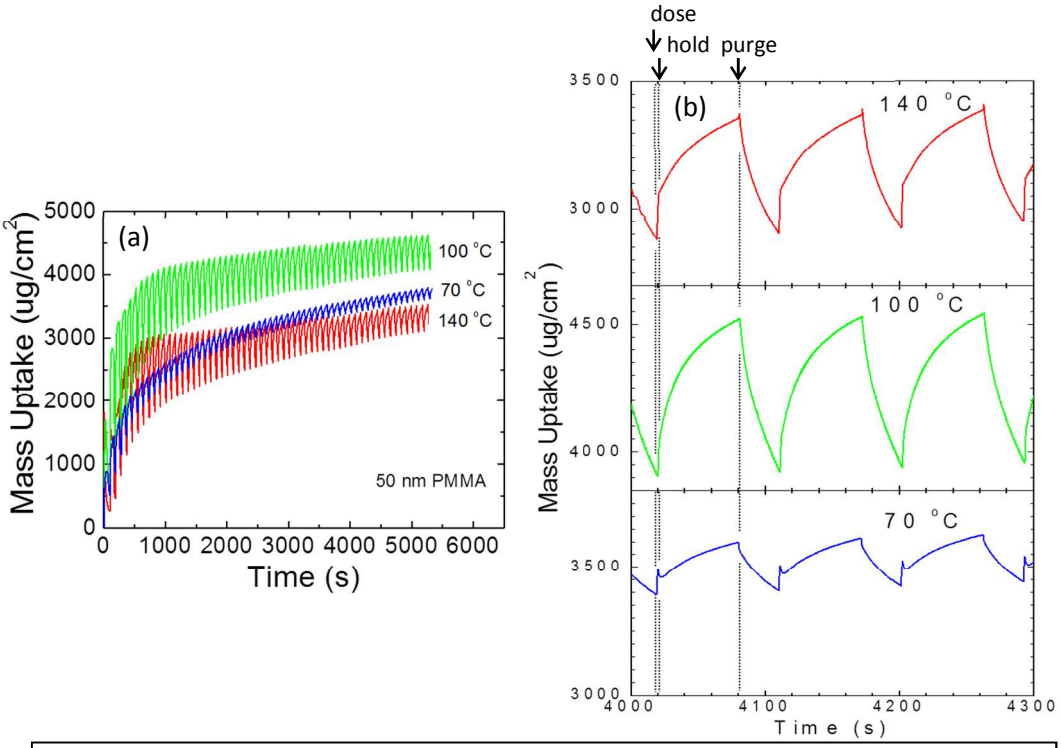

Figure 2. (a) Overall QCM mass response for 50 nm PMMA films exposed to 100 TMA doses at 70, 100 and 140 °C. (b) Magnified view of the mass response after ~80 TMA doses.

temperatures shown the net mass uptake is largest at 100 °C. Each TMA dose produces mass uptake followed by mass loss. The traces collected during TMA doses 41-43 (Fig. 2b) show that after the initial mass uptake the mass loss is nearly equal to the mass gain, with the largest gain and loss at 100 °C. The trace shape also varies with temperature. At 140 °C the mass gain jumps rapidly then continues more slowly. At 100 °C the mass increases continuously, whereas at 70 °C the mass uptake shows a peak followed by a small loss before continuing to grow. The QCM traces show TMA uptake and loss from the

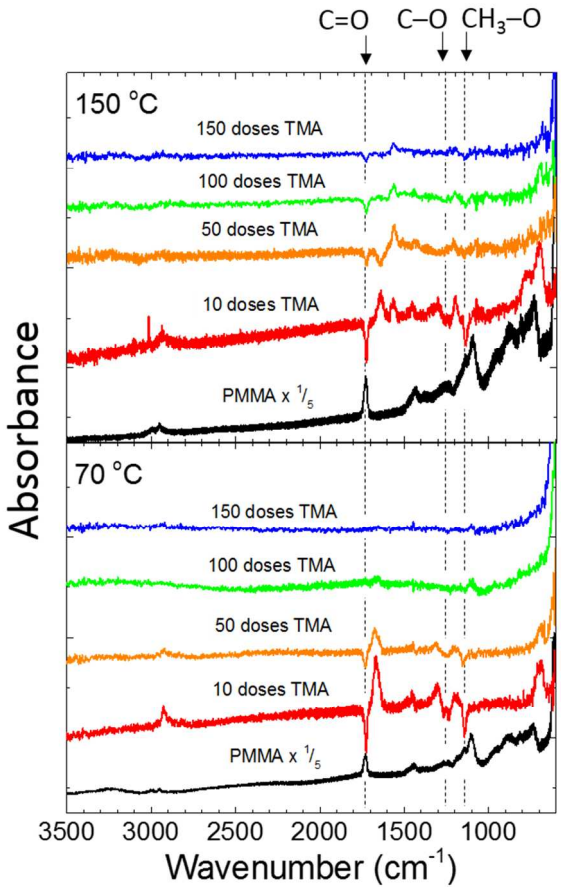

Figure 3. *In situ* FTIR data collected at 70 and 150 °C at several times during 150 TMA/purge dose steps. Each differential spectrum is referenced to the preceding spectrum shown. The data shows different reaction trends at different temperatures, most noticeably in the region between 1500 and 1700 cm^{-1}.

PMMA bulk during each hold/purge step. The trace shape at 70 °C is ascribed to relatively small amounts of TMA rapidly adsorbing and desorbing on the film surface, combined with slower TMA diffusion in and out of the PMMA bulk. Also, using QCM we find that after 50 dose steps at 70 °C a long (85 min) purge leads to a loss of 60 % of the mass gained, whereas the same experiment at 150 °C leads to a mass loss of around 30 %. At 150 °C the mass loss plateaued after purging for approximately 15 minutes; at 70 °C the mass loss did not plateau during the extended purge. This mass uptake/loss during

TMA exposure on polymers, including PMMA, has been observed[9] but has not previously been analyzed as a function of process temperature.

To further understand the trend in mass uptake versus exposure and temperature, we measured *in situ* IR absorbance versus TMA exposure at 70 and 150 °C, as shown in Figure 3. The figure shows difference spectra relative to the previously plotted spectrum, where negative-going features correspond to modes removed and positive-going features are modes added. The spectrum labeled "10 doses TMA" corresponds to changes that occur between 0 and 10 doses, whereas "50 doses TMA" shows changes between 10 and 50 doses. Considering the data collected at 70 °C we see large changes during the first 10 doses including: loss of C=O stretching at 1732 cm^{-1}; loss of C-O at 1260 and 1143 cm^{-1}; and gains at 1670, 1305, and 1200 cm^{-1}. This change continues, but is less pronounced for the next 40 doses with only small changes appearing after 100 and 150 TMA doses. At 150 °C, these same changes are observed with the addition of a new mode appearing at 1568 cm^{-1} after 10 doses (also seen in Figure 1) which is not observed at 70 °C. After 40 more TMA doses at 150 °C the spectrum shows a further decrease at 1732 cm^{-1}. The mode at 1670 cm^{-1}, is now negative-going with an increase at 1568 cm^{-1}. Note that the feature at 1670 cm^{-1} that disappeared after 50 TMA doses at 150 °C is the same mode that appeared during the first 10 doses at both 150 and 70 °C. The degradation of the 1670 cm^{-1} mode during TMA exposure is only observed at elevated temperature in our experiments. This trend, peak appearance followed by its disappearance, indicates the formation of a metastable intermediate (mode at 1670 cm^{-1}) that reacts at elevated temperature to create a more stable product state with a C=O mode at 1568 cm^{-1}. Between 50 and 150 TMA doses we continue to observe loss of the PMMA C=O mode at 1732 cm^{-1} and corresponding gain in the 1568 cm^{-1} feature consistent with stable product formation at the higher temperature.

Quantum Chemical Analysis

We performed quantum chemistry calculations as described above to minimize the potential energy for a PMMA analog, TMA and various possible reaction-product states. Figure 4 shows chemical structures for the species modeled, and the corresponding vibrational spectra. The calculated spectrum for the PMMA model (Fig. 4a) shows peaks at 1790, 1307, 1212 and 1182 cm^{-1}. The peak at 1790 cm^{-1} results from C=O stretch, and the other three peaks correspond to coupled =C-O- and -O-CH_3 stretching modes. Carbon-hydrogen stretching and deformation modes are also present at 3000-3200 and 1400-1550 cm^{-1}, respectively. The starting PMMA spectrum in Figure 1 shows a peaks 1732 cm^{-1} (C=O stretch), and at 1260 and 1143 cm^{-1} (=C-O- and -O-CH_3 stretch).[21] Table 1 lists the experimentally observed and calculated peak positions (as output and after frequency adjustment) for PMMA before and after TMA exposure. For the starting PMMA, the calculated peaks match well with the experimental values. An additional peak predicted near 1165 cm^{-1} is not distinctly observed, but it could correspond to a shoulder that appears near 1189 cm^{-1} on the 1143 cm^{-1} peak.

Previous quantum chemistry analysis of TMA interacting with surface hydroxyls during TMA/water ALD shows that TMA forms a short-lived metastable -O···$Al(CH_3)_3$ adduct that subsequently reacts exothermically to yield stable -O-$Al(CH_3)_2$ and methane.[22] Also, since TMA is a strong Lewis acid[23], we minimized the energy for TMA physisorbed to the C=O through a Lewis acid/base adduct state, producing the structure and corresponding vibrational spectrum shown in Figure 4. Like the experimental results, the calculated spectrum was plotted relative to the starting PMMA. The calculated spectrum for PMMA+TMA shows negative-going modes at 1790, 1307, 1212 and 1182 cm^{-1} and new positive-going features at 1725, 1323, 1237 and 1197 cm^{-1}. A peak near 730 cm^{-1} corresponds to Al-methyl rocking modes in the Al-CH_3 groups. The Gaussview model confirms that the 1725 cm^{-1} peak corresponds to stretching of the C=O unit coordinated with $Al(CH_3)_3$. Likewise the 1323, 1237 and 1197 cm^{-1} peaks correspond to =C-O- and -O-CH_3 coupled vibrations neighboring the -C=O···$Al(CH_3)_3$ coordinated structure. A shift in the C=O frequency to smaller wavenumber is expected with an increase

in the C=O bond length, which is consistent with TMA coordination. The coordination will also change the =C-O- and -O-CH_3 bond lengths, shifting the mode frequencies. These modes are expected to appear in the experimental spectra near 1658, 1271, 1189, and 1150 cm^{-1}, respectively, as indicated in Table 1.

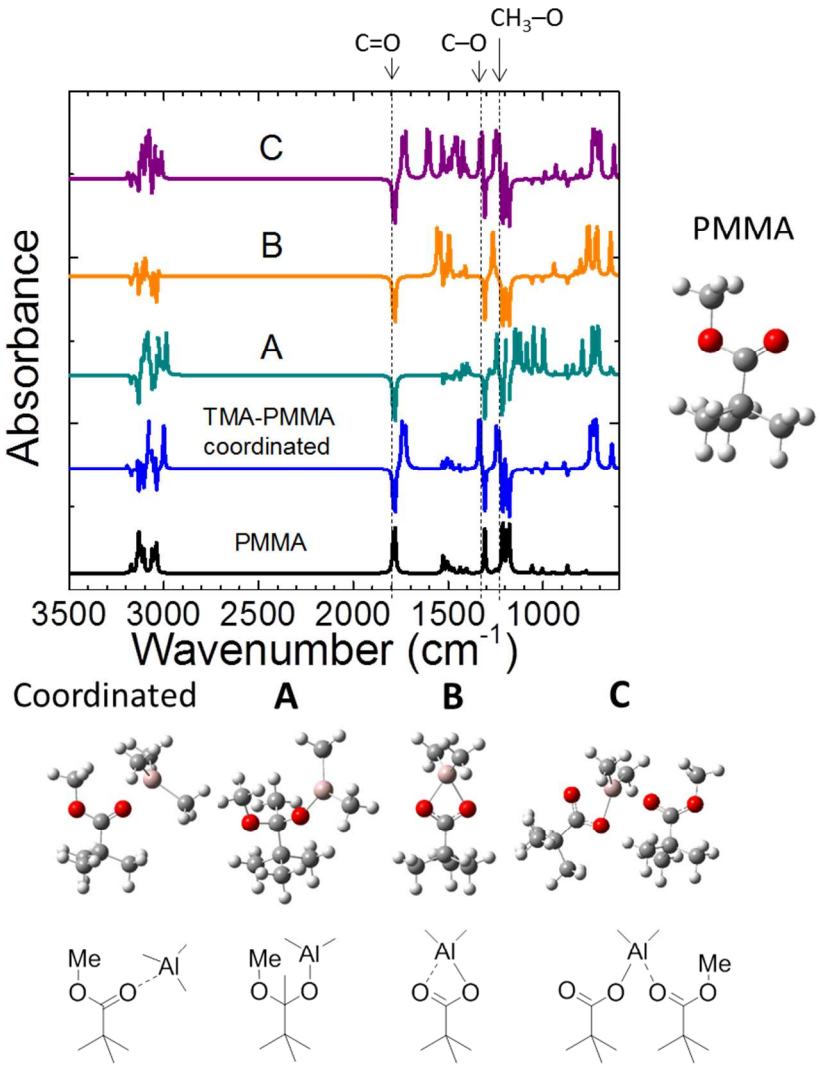

Figure 4. Relaxed chemical structures calculated using *ab initio* modeling, and their corresponding vibrational spectra referenced to spectra from structures calculated without TMA interaction. The bond models used for the calculations are also shown. The calculated spectrum for the PMMA model shows peaks at 1790 cm^{-1} corresponding to C=O stretch, and features at 1307, 1212 and 1182 cm^{-1} associated with =C-O- and -O-CH_3 coupled modes. For each structure, interaction with TMA leads to loss of the 1790 cm^{-1} C=O mode and changes in the C-O vibrations. The peak at 1725 cm^{-1} is TMA coordinated to the C=O in a physisorbed state, and is consistent with the IR and QCM results at lower temperature. Peaks between 1750 and 1500 cm^{-1} in products **B** and **C** correspond to C=O coordinated with a neighboring covalently-bound Al-O, forming a resonant C=O···Al-O-C unit, consistent with the higher temperature product mode observed at 1568 cm^{-1}.

The experimental data collected at 70 °C shows three clear positive-going modes at 1670, 1305, and 1200 cm^{-1} after TMA exposure. As in the PMMA spectrum before TMA exposure, the calculated peak near 1150 cm^{-1} is not readily observed. The predicted peaks after TMA exposure are at generally smaller wavenumber than experimentally observed, i.e. the errors between the adjusted and measured peak positions are somewhat larger after TMA exposure than for neat PMMA. Since the calculations do not include thermal or matrix effects, and the base cluster size utilized was relatively small, we expect the calculation to exaggerate the interaction, shifting the peaks more than experimentally measured. With this consideration, the adjusted peaks agree well with the experimental values. The other frequencies included in Table 1 are discussed below.

Observed Chromatic Shift

Bulk PMMA powder was exposed to TMA vapor at 90 and 150 °C in a fiber-encapsulated basket placed inside our reaction chamber, as previously described.[24] PMMA powder as received is white, as

Material	Experiment	Calculated	Adjusted [a]	Vibration
PMMA	1732 cm^{-1}	1790 cm^{-1}	1720 cm^{-1}	C=O
	1260	1307	1256	=C-O- and -O-CH_3
	--	1212	1165	
	1143	1182	1136	
PMMA + TMA	1670	1725	1658	C=O···Al-$(CH_3)_3$
	1305	1323	1271	=C-O- and O-CH_3 with C=O···Al$(CH_3)_3$
	1200	1237	1189	
	--	1197	1150	
	1568	1605[b]	1542[b]	C=O with =C-O-Al$(CH_3)_2$

Table 1. Experimental, calculated and adjusted IR peak positions for methyl trimethylacetate as a model for PMMA. Experimental and calculated peak positions are also shown for the starting material after exposure to trimethylaluminum. [a]The scaling factor used was 0.961. [b]Calculated and adjusted values are from structure **C** in Figure 4, a simplified version of the product shown in Figure 6. All values are in cm^{-1}.

shown in Figure 5a. Upon 600 TMA doses at 90 °C, no color change was observed. When the reactor temperature was increased to 150 °C, the powder appeared black upon removal from the reactor. Faint popping sounds could be heard as the black powder converted to orange, consistent with a rapid reaction between the TMA–PMMA composite and water in the air. After 24 hours the powder was reddish brown. The sample maintained a stable orange color for more than 9 months following exposure, as shown in Figure 5f. Color changes due to metal atoms bonded and coordinated to organic groups are often used as metal-complex dyes.[25] Complex-dyes have structures similar to that of alumina bound to multiple PMMA pendent groups as depicted in Figure 4c.

Discussion

Based on the IR and QCM data combined with the *ab initio* analysis results, we conclude that

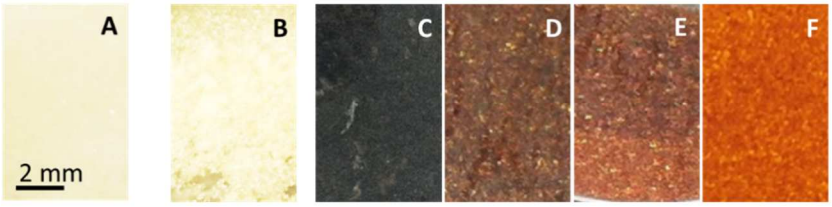

Figure 5. Bulk PMMA powder, as received, was treated with 600 TMA doses at varying temperatures. At increased temperatures a color change was observed that was not seen at lower temperatures. A) PMMA powder as received. B) PMMA powder with 600 SVI TMA doses at 90 ^{o}C. C) PMMA powder with 600 SVI TMA doses at 150 ^{o}C immediately after removal from the reactor, after D) 1.5 hrs E) 24 hrs and F) 9 months.

over a wide temperature range TMA diffuses into the polymer bulk and forms a metastable adduct, coordinating to the PMMA ester carbonyl. The physisorbed TMA shifts the C=O stretching frequency from 1732 to 1670 cm^{-1}, which appears in the difference spectra in Figure 1 as a mode loss adjacent to a mode gain. By interaction with the carbonyl oxygen, the TMA Lewis acid increases the C=O bond length and decreases the stretching frequency. The change in the C=O unit also draws some charge from the =C-O- and -O-CH$_3$ bonds, shifting the modes at 1260 and 1143 cm^{-1}.

At low temperature, TMA can desorb from the C=O···Al(CH_3)$_3$ complex, as shown in the QCM results, and subsequent water exposure leads to relatively small changes in the starting PMMA. At high temperature, the physisorbed structure converts to form a PMMA–TMA reaction product with a characteristic vibration at 1568 cm^{-1}. This reaction proceeds relatively rapidly at higher temperature (within the first 10 TMA doses at 150 °C, Figure 3). Moreover, the PMMA–TMA reaction product is stable; the IR data in Figure 1 shows that it remains present after water exposure.

The QCM results (Fig. 2) also show TMA uptake in the PMMA bulk, followed by desorption.

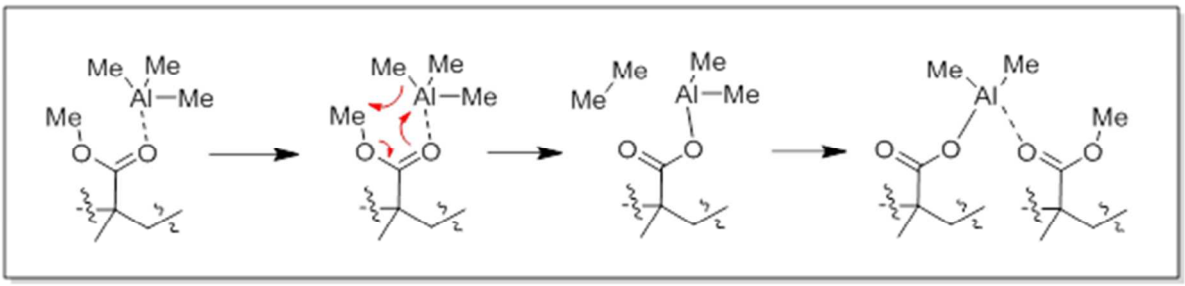

Figure 6. Proposed pericyclic activation of ester to form metal acetate.

QCM analysis on a planar quartz crystal substrate typically shows a mass uptake of ~40 ng/cm^2 per cycle during steady-state TMA/water ALD.[26,27] We find that at 100 °C, one TMA dose onto PMMA produces a mass change > 500 ng/cm^2. This large mass change is ascribed to TMA diffusing into the polymer bulk. This sub-surface diffusion of ALD precursors into several different polymers has been previously observed by IR, QCM, TEM and other methods. We also note that the magnitude of overall mass uptake after 150 TMA doses (Fig 2a) increases with temperature between 70 and 100 °C, but it is not as large at 140 °C. At low temperature, where IR indicates that TMA does not react with PMMA, increasing the temperature will promote TMA diffusion. At high-temperature, reaction between TMA and PMMA will fix TMA and therefore slow sub-surface diffusion. Therefore, the temperature-dependent QCM results further support the TMA adsorption–desorption and reaction mechanism described above.

We now consider possible PMMA–TMA reaction products that could account for the observed data, including the characteristic IR vibration at 1568 cm^{-1}. One product we considered is structure **A** in Figure 4. This could be produced by breaking the carbonyl to form Al-O, transferring a methyl to the carbon. Even though this product was previously considered,[12] this reaction scheme is not likely because methyl migration products from TMA adducts typically require stronger electron donating functional groups than ester carbonyls.[28] Even so, we performed a geometry optimization for this structure and examined its vibrational modes using Gaussian, the resulting spectrum is plotted in Figure 4. The carbonyl stretch is lost and new C-O coupled modes appear between 1000 and 1300 cm^{-1}. No new modes appear in the 1500-1700 cm^{-1} region where the stable product is experimentally observed. Since this product lacks the vibrational signature of the resulting product, and because the reaction scheme is not favorable, we looked for other possible stable products.

Another possibility, shown as structure **B** in Figure 4, is that the TMA in the coordination complex interacts with the neighboring methoxy group in a pericyclic reaction to yield a covalent bond between $Al(CH_3)_2$ and the oxygen originally in the carbonyl. The methyl lost from the TMA reacts with the methoxy moiety forming ethane vapor and an ester carbonyl. The proximal Al center would then coordinate to the carbonyl oxygen in the same ester, as shown in product **B**, or in a neighboring ester as shown in product **C** and in Figure 6. The reaction scheme in Figure 6 is energetically driven by formation of the strong Al-O and ethane bonds. The scheme is consistent with the relative stability of TMA reacting with esters, where TMA/ester complexes are known to catalyze Tischenko-like reduction of *beta*-ketoesters without degradation of the ester moiety.[28,29] These pericyclic reactions are common in organic/inorganic complex formation and in other synthetic routes where TMA is able to promote methyl translation to form C-C bonds.[30] Since products **B** and **C** are synthetically feasible, we considered them further for *ab initio* modeling. Figure 4 shows the minimized structures and characteristic vibrational spectra. Both products **B** and **C** show loss of the C=O and coupled C-O stretching in the

starting PMMA. Most notably, new modes appear in the 1500 -1700 cm^{-1} region that correspond to C=O stretching modes shifted to lower frequency due to Al coordination and near-neighbor bonding. In product **B**, the model constrains the Al coordination and bonding on the same ester unit and modes appear at 1520 and 1480 cm^{-1}. For product structure **C**, Al binds to adjacent esters, producing a C=O stretch that is red-shifted to 1605 cm^{-1}. In highly TMA-saturated PMMA, further reactions between -O-$Al(CH_3)_2$ and other esters would form additional bond/coordination pairs, leading to further mode shifting. Based on this result, we believe that the mode at 1568 cm^{-1} arises from C=O stretching vibrations where the carbonyl carbon is also linked to -O-$Al(CH_3)_2$ (or possibly -O-$Al(CH_3)$-O-) with the Al further coordinated with oxygen on other chains, as depicted in Figure 6. To further support this scheme, we note that PMMA powder, that appears white as received, remains visibly unchanged after TMA exposure at low temperature, whereas TMA exposure at high temperature leads to a dramatic, visible color change to black that transitions to orange upon exposure to air. This coloration may therefore be due to products where the metal atom bridges multiple organic groups, as commonly found in metal-complexed dyes.[25] The color shift could be attributed to atmospheric water slightly altering the metal-organic structure; the permanence of this color change attests to the stability of this final product.

Summary

Combining evidence from *in situ* infrared transmission, quartz crystal microbalance experiments and *ab initio* modeling analysis, we conclude that exposing TMA vapor to PMMA thin films leads to significant subsurface TMA infiltration where the TMA physisorbs onto C=O forming a metastable C=O···$Al(CH_3)_3$ structure. Upon TMA physisorption, the PMMA C=O stretching frequency at 1732 cm^{-1} shifts to 1670 cm^{-1} when the TMA Lewis base withdraws electrons from the C=O bond. At low temperatures (up to ~100 °C), the interaction does not produce C-O-Al covalent bonds[12] and the TMA readily desorbs. At higher temperatures an IR feature near 1568 cm^{-1} arises, likely due to C=O stretching

in resonant C=O···Al-O-C units. These bonds could possibly form through a pericyclic reaction involving a PMMA methoxy group interacting with a neighboring TMA stabilized through coordination with the C=O ester. This improved understanding of the mechanisms for TMA interaction with PMMA will also extend to other polymers and other Lewis acidic metal-vapor reactants, helping to create knowledge and advance applications for sequential vapor infiltration processes.

Acknowledgment

The authors acknowledge support from NSF project # 1344618 and from Lam Research Corporation. One co-author (C.D.N.) acknowledges support from the US Dept. of Education under the GAANN Fellowship program, project P200A09008.

References

(1) Lee, S.-M.; Pippel, E.; Gosele, U.; Dresbach, C.; Qin, Y.; Chandran, C. V.; Brauniger, T.; Hause, G.; Knez, M. Greatly Increased Toughness of Infiltrated Spider Silk. *Science* **2009**, *324*, 488–492.

(2) Lee, S.-M.; Pippel, E.; Moutanabbir, O.; Gunkel, I.; Thurn-Albrecht, T.; Knez, M. Improved Mechanical Stability of Dried Collagen Membrane after Metal Infiltration. *ACS Appl. Mater. Interfaces* **2010**, *2*, 2436–2441.

(3) Spagnola, J. C.; Gong, B.; Arvidson, S. A.; Jur, J. S.; Khan, S. A.; Parsons, G. N. Surface and Sub-Surface Reactions during Low Temperature Aluminium Oxide Atomic Layer Deposition on Fiber-Forming Polymers. *J. Mater. Chem.* **2010**, *20*, 4213–4222.

(4) Gong, B.; Peng, Q.; Jur, J. S.; Devine, C. K.; Lee, K.; Parsons, G. N. Sequential Vapor Infiltration of Metal Oxides into Sacrificial Polyester Fibers: Shape Replication and Controlled Porosity of Microporous/Mesoporous Oxide Monoliths. *Chem. Mater.* **2011**, *23*, 3476–3485.

(5) Peng, Q.; Tseng, Y.-C.; Darling, S. B.; Elam, J. W. Nanoscopic Patterned Materials with Tunable Dimensions via Atomic Layer Deposition on Block Copolymers. *Adv. Mater.* **2010**, *22*, 5129–5133.

(6) Peng, Q.; Tseng, Y.-C.; Darling, S. B.; Elam, J. W. A Route to Nanoscopic Materials via Sequential Infiltration Synthesis on Block Copolymer Templates. *ACS Nano* **2011**, *5*, 4600–4606.

(7) Tseng, Y.-C.; Peng, Q.; Ocola, L. E.; Elam, J. W.; Darling, S. B. Enhanced Block Copolymer Lithography Using Sequential Infiltration Synthesis. *J. Phys. Chem. C* **2011**, *115*, 17725–17729.

(8) Akyildiz, H. I.; Padbury, R. P.; Parsons, G. N.; Jur, J. S. Temperature and Exposure Dependence of Hybrid Organic-Inorganic Layer Formation by Sequential Vapor Infiltration into Polymer Fibers. *Langmuir* **2012**, *28*, 15697–15704.

(9) Wilson, C. A.; Grubbs, R. K.; George, S. M. Nucleation and Growth during Al2O3 Atomic Layer Deposition on Polymers. *Chem. Mater.* **2005**, *17*, 5625–5634.

(10) Farm, E.; Kemell, M.; Ritala, M.; Leskela, M. Selective-Area Atomic Layer Deposition Using Poly(methyl Methacrylate) Films as Mask. *J. Phys. Chem. C* **2008**, *112*, 15791–15795.

(11) Parsons, G. N.; George, S. M.; Knez, M. Progress and Future Directions for Atomic Layer Deposition and ALD-Based Chemistry. *MRS Bull.* **2011**, *36*, 865–871.
(12) Gong, B.; Parsons, G. N. Quantitative in Situ Infrared Analysis of Reactions between Trimethylaluminum and Polymers during Al2O3 Atomic Layer Deposition. *J. Mater. Chem.* **2012**, *22*, 15672–15682.
(13) Jur, J. S.; Spagnola, J. C.; Lee, K.; Gong, B.; Peng, Q.; Parsons, G. N. Temperature-Dependent Subsurface Growth during Atomic Layer Deposition on Polypropylene and Cellulose Fibers. *Langmuir* **2010**, *26*, 8239–8244.
(14) Gong, B.; Kim, D. H.; Parsons, G. N. Mesoporous Metal Oxides by Vapor Infiltration and Atomic Layer Deposition on Ordered Surfactant Polymer Films. *Langmuir* **2012**, *28*, 11915–11922.
(15) Frisch, M. J.; Trucks, G. W.; Schlegel, H. B.; Scuseria, G. E.; Robb, M. A.; Cheeseman, J. R.; Scalmani, G.; Barone, V.; Mennucci, B.; Petersson, G. A.; Nakatsuji, H.; Caricato, M.; Li, X.; Hratchian, H. P.; Izmaylov, A. F.; Bloino, J.; Zheng, G.; Sonnenberg, J. L.; Hada, M.; Ehara, M.; Toyota, K.; Fukuda, R.; Hasegawa, J.; Ishida, M.; Nakajima, T.; Honda, Y.; Kitao, O.; Nakai, H.; Vreven, T.; Montgomery, J. A., Jr.; Peralta, J. E.; Ogliaro, F.; Bearpark, M.; Heyd, J. J.; Brothers, E.; Kudin, K. N.; Staroverov, V. N.; Kobayashi, R.; Normand, J.; Raghavachari, K.; Rendell, A.; Burant, J. C.; Iyengar, S. S.; Tomasi, J.; Cossi, M.; Rega, N.; Millam, N. J.; Klene, M.; Knox, J. E.; Cross, J. B.; Bakken, V.; Adamo, C.; Jaramillo, J.; Gomperts, R.; Stratmann, R. E.; Yazyev, O.; Austin, A. J.; Cammi, R.; Pomelli, C.; Ochterski, J. W.; Martin, R. L.; Morokuma, K.; Zakrzewski, V. G.; Voth, G. A.; Salvador, P.; Dannenberg, J. J.; Dapprich, S.; Daniels, A. D.; Farkas, Ö.; Foresman, J. B.; Ortiz, J. V.; Cioslowski, J.; Fox, D. J. Gaussian 09, Revision D.01. *Gaussian Inc Wallingford CT* **2009**.
(16) Wong, M. W. Vibrational Frequency Prediction Using Density Functional Theory. *Chem. Phys. Lett.* **1996**, *256*, 391–399.
(17) Scott, A. P.; Radom, L. Harmonic Vibrational Frequencies: An Evaluation of Hartree−Fock, Møller−Plesset, Quadratic Configuration Interaction, Density Functional Theory, and Semiempirical Scale Factors. *J. Phys. Chem.* **1996**, *100*, 16502–16513.
(18) Dennington, R.; Keith, T.; Millam, J. *GaussView*; Semichem Inc.: Shawnee Mission KS, 2009.
(19) Naito, K.; Johnson, G. E.; Allara, D. L.; Kwei, T. K. Compatibility in Blends of Poly(methyl Methacrylate) and Poly(styrene-Co-Acrylonitrile). 1. Physical Properties. *Macromolecules* **1978**, *11*, 1260–1265.
(20) When this article was originally submitted, similar findings regarding the PMMA C=O/TMA Lewis acid/base adduct and related IR spectra were independently reported: Mahua Biswas; Joseph A. Libera; Seth B. Darling; and Jeffrey W. Elam. Nanopatterning of Inorganic Materials by Sequential Infiltration Synthesis: In Situ FTIR Investigation of the Precursor-Polymer Interaction. In *2014 AVS Topical Conference on Atomic Layer Deposition (ALD 2014)*; Kyoto, Japan, June 18, 2014; AVS, Chico CA (2014).
(21) Noda, I.; Dowrey, A. E.; Haynes, J. L.; Marcott, C. Group Frequency Assignments for Major Infrared Bands Observed in Common Synthetic Polymers. In *Physical Properties of Polymers Handbook*; Mark, J. E., Ed.; Springer New York, 2007; pp. 395–406.
(22) Xu, Y.; Musgrave, C. B. A DFT Study of the Al2O3 Atomic Layer Deposition on SAMs: Effect of SAM Termination. *Chem. Mater.* **2004**, *16*, 646–653.
(23) M. Witt; H.W. Roesky. Organoaluminum Chemistry at the Forefront of Research and Development. *Curr Sci* **2000**, *78*, 410.
(24) Devine, C. K.; Oldham, C. J.; Jur, J. S.; Gong, B.; Parsons, G. N. Fiber Containment for Improved Laboratory Handling and Uniform Nanocoating of Milligram Quantities of Carbon Nanotubes by Atomic Layer Deposition. *Langmuir* **2011**.
(25) *Ullmann's Encyclopedia of Industrial Chemistry*; Wiley-VCH Verlag GmbH & Co. KGaA, Ed.; Wiley-VCH Verlag GmbH & Co. KGaA: Weinheim, Germany, 2000.

(26) J.W. Elam; M.D. Groner; S.M. George. Viscous Flow Reactor with Quartz Crystal Microbalance for Thin Film Growth by Atomic Layer Deposition. *Rev Sci Instrum.* **2002**, *73*, 2981–2987.
(27) Rocklein, M. N.; George, S. M. Temperature-Induced Apparent Mass Changes Observed during Quartz Crystal Microbalance Measurements of Atomic Layer Deposition. *Anal. Chem.* **2003**, *75*, 4975–4982.
(28) Donald Craig; Fredrick W. Goldberg; Richard W. Pett; Niels T.H. Tholen; Andrew J. P. White. Aziridine-Based Concise Synthesis of (+-)-Alstonerine. *Chem. Commun.* **2013**, *49*, 9275.
(29) S. Sano; H. Shimizu; Y. Nagao. Trimethylaluminium-Induced Diastereoselective Methylation onto Ethyl 2-Oxocyclopentane-1-Carboxylate and Isomerization between the Dimethylaluminium-Alkoxide Products. *Tetrahedron Lett.* **2005**, *46*, 2887–2891.
(30) Kazuhiko Takai; Ichiro Mori; Koichiro Oshima; Hitosi Nozaki. Aliphatic Claisen Rearrangement Promoted by Organoaluminum Reagents. *Bull Chem Soc Jpn* **1984**, *57*, 446–451.